Received: 14 July 2016 | Accepted: 30 December 2016

DOI: 10.1111/jace.14767

ORIGINAL ARTICLE

Journal of the American Ceramic Society

In situ crystallization and elastic properties of transparent $MgO–Al_2O_3–SiO_2$ glass-ceramic

Leonardo Sant'Ana Gallo[1,2] | Fabrice Célarié[2] | Nathalie Audebrand[3] | Ana Candida Martins Rodrigues[1] | Edgar Dutra Zanotto[1] | Tanguy Rouxel[2]

[1]Vitreous Materials Laboratory - LaMaV, Materials Engineering Department - DEMa, Federal University of São Carlos, São Carlos, São Paulo, Brazil

[2]Département Mécanique et Verres, IPR UMR UR1-CNRS 6251 - Université de Rennes 1, Rennes, France

[3]Institut des Sciences Chimiques Rennes, UMR CNRS 6226 - Université de Rennes 1, Rennes, France

Correspondence
Leonardo Sant'Ana Gallo, Vitreous Materials Laboratory-LaMaV, Materials Engineering Department-DEMa, Federal University of São Carlos, São Carlos, São Paulo, Brazil.
Email: leonardo.s.gallo@gmail.com
Tanguy Rouxel, Département Mécanique et Verres, IPR UMR UR1-CNRS 6251-Université de Rennes 1, Rennes, France.
Email: tanguy.rouxel@univ-rennes1.fr

Funding information
Fundação de Amparo à Pesquisa do Estado de São Paulo, Grant/Award Number: 2013/07793-6, 2014/03004-0; Center for Research, Technology and Education in Vitreous, Grant/Award Number: 2013/07793-6; European Research Council, Grant/Award Number: 320506.

Abstract

Glass-ceramics (GC) generally possess enhanced mechanical properties compared to their parent glasses. The knowledge of how crystallization evolves and affects the mechanical properties with increasing temperature is essential to optimize the design of the crystallization cycle. In this study, we crystallized a glass of the $MgO–Al_2O_3–SiO_2$ system with nucleating agents TiO_2 and ZrO_2. The crystallization cycle comprised a 48 hour nucleation treatment at the glass-transition temperature followed by a 10 hour growth step at a higher temperature. During this cycle, the evolution of crystalline phases was followed by high-temperature X-ray diffraction (HTXRD), which revealed the presence of karooite ($MgO{\cdot}2TiO_2$), spinel ($MgO{\cdot}Al_2O_3$), rutile (TiO_2), sillimanite ($Al_2O_3{\cdot}SiO_2$), and sapphirine ($4MgO{\cdot}5Al_2O_3{\cdot}2SiO_2$). The same heat treatment was applied for in situ measurement of elastic properties: elastic modulus, E, shear modulus, G, and Poisson's ratio, ν. The evolution of these parameters during the heating path from room temperature to the final crystallization temperature and during the nucleation and the crystallization plateaus is discussed. E and G evolve significantly in the first two hours of the growth step. At the end of the crystallization process, the elastic and shear moduli of the GC were approximately 20% larger than those of the parent glass.

KEYWORDS
crystallization, elastic constants, glass-ceramics, mechanical properties

1 | INTRODUCTION

Glass-ceramics (GC) are high-tech polycrystalline materials obtained by controlled crystallization of certain glasses. GC can be used in a wide range of applications,[1] such as bioactive materials for bone replacement,[2,3] optical materials,[4] dental components,[5] and mechanically resistant devices.[6-9] Crystallization may occur in a homogeneous or heterogeneous manner.[10] Heterogeneous nucleation is more likely to occur than homogeneous nucleation because the corresponding surface energy is minimized at certain nucleation sites. Volumetric heterogeneous nucleation is normally favored with the aid of nucleating agents. Different microstructures obtained through controlled crystallization may lead to distinct mechanical properties. For instance, Serbena et al.[11] have shown that different volume fractions of lithium disilicate crystals embedded in an isochemical glass matrix lead to widely different values of fracture toughness, K_{IC}. Also, Peitl et al.[2] have shown that the fracture strength of a bioactive

Presented at the 11th International Symposium on Crystallization in Glasses and Liquids, Nagaoka, Japan. October 14, 2015 (Paper No. O37)

glass increases up to a crystallized volume fraction of 40-50; it then remains constant with further increase in the crystallized volume fraction. $MgO–Al_2O_3–SiO_2$ (MAS) glass is an example of a system that can lead to strong glass-ceramics[12–16] with the aid of nucleating agents, such as TiO_2[17,18] or ZrO_2,[17,19,20] but others such as Fe_2O_3[21] and V_2O_5[22] have also been used. However, these last two oxides impart strong colors to the material.

In this study, a carefully controlled double-stage heat treatment was designed and used to crystallize a glass of the MAS system with TiO_2 and ZrO_2 added as the nucleating agents to promote thinly and uniformly dispersed crystals in the glass matrix. The objective was to develop an adequate composition and optimize the thermal treatment to produce a transparent, hard, lightweight glass-ceramic. The relative low density (~2.7 g/cm^3) of cordierite when compared with other ballistic-protection materials (3.5-5.0 g/cm^3) and the possibility to obtain a transparent GC are the main reasons for which this system was chosen.

The importance of the MAS glasses for the current research lies in the fact that they may potentially crystallize hard phases of low density, such as cordierite ($2MgO.2Al_2O_3.5SiO_2$) and sapphirine ($4MgO.5Al_2O_3.2SiO_2$). Thus, with an adequate heat-treatment MAS glasses may yield lightweight, strong, transparent glass-ceramics. These glass-ceramics are intended to be used as a protective material to block high kinetic-energy blasts. Whether they are transparent or not, glass-ceramics are an interesting alternative to the traditionally employed ceramics for ballistic protection. They are generally less dense than polycrystalline alumina ($\rho_{Al_2O_3} = 3.95$ g/cm^3;[23]), much less expensive than non-oxide ceramics, and less expensive to produce than transparent ceramics, such as sapphire, spinel $MgO.Al_2O_3$, or $(AlN)_2O_3$.

GC compositions containing lithium disilicate ($Li_2O·2SiO_2$–LS2) as the main crystalline phase have been tested as ballistic protection.[6–8,24–27] They can present hardness up to 635 HK[6] and fracture toughness, K_{IC}, of 3.3 MPa.m$^{1/2}$;[28] Glass-ceramics of the MAS system can present higher hardness and elastic modulus than those of LS2. Those properties, combined with low density, make them good candidates for ballistic-protection materials.

Shao et al.[12] crystallized a glass composition on the MAS system, having TiO_2 as nucleating agent. They applied a 2-hour heat treatment on six different temperatures and depending on the temperature, the crystal phases formed after crystallization were alpha- and beta-quartz solid solutions, cordierite, and sapphirine. The highest hardness reported was 8.5 GPa and the highest Young's Modulus was 137 GPa, both for a sample heat-treated at 1100°C, which had alpha-cordierite, alpha-quartz, and sapphirine, as crystal phases.

Dittmer and Rüssel[29] studied different glass compositions of the MAS system with the addition of ZrO_2 as a nucleating agent. Some compositions had also additions of ZnO and P_2O_5. A glass composition having 7 mol% of nucleating agent was reported to present, after a heat treatment at 1150°C for 3 hour, an impressive hardness of 13.3 GPa and K_{IC} of 2.7 MPa·m$^{1/2}$. Höland and Beall's book[1] can be referred for more information on glass-ceramics of this system.

In this work, the appearance of crystalline phases was monitored by in situ high-temperature X-ray diffraction during nucleation and crystal growth treatments of several hours. The evolution of the elastic properties was also characterized in situ using a mechanical resonance technique. Observed changes in the elastic (E) and shear (G) moduli and in the Poisson's ratio (ν) are discussed.

These in situ measurements are useful to specify the necessary duration of heat treatments to attain the optimized mechanical properties at the corresponding temperature. This optimization is important for commercial glasses because all the production steps must be carefully designed to minimize cost. Although this type of study has already been conducted on different systems,[30] and despite the importance of the MAS system and the numerous related articles, the in situ measurements described here are, to the best of our knowledge, the first of this type performed for MAS glass-ceramics.

2 | EXPERIMENTAL PROCEDURE

2.1 | Glass composition and sample preparation

The studied nominal glass composition is shown in Table 1. This composition was designed to correspond to a nominal mixture of 75 mol% cordierite ($2MgO·2Al_2O_3·5SiO_2$) and 25 mol% of a residual glassy matrix consisting of glass formers (B_2O_3 and SiO_2) a fining agent (Sb_2O_3) and the nucleating agents (TiO_2 and ZrO_2). Al_2O_3 (purity>98%), SiO_2 (>99%), B_2O_3 (>98%), TiO_2 (>98%), and Sb_2O_3 (>98%) were purchased from Sigma-Aldrich (Saint Louis, MO, USA), and MgO (purity>98%) and ZrO_2 (>99%) were purchased from Acros Organics (Geel, Antwerp, Belgium). The concentration of nucleating agents was chosen after a study of Fokin and Zanotto,[31] where a series of MAS-cordierite glasses having different amounts of TiO_2 were prepared. Bulk nucleation was observed only in a glass having 6.9 mol% of TiO_2. Lower amounts resulted in surface nucleation. ZrO_2 was added in a minor scale since it is generally poorly soluble on molten silicates. B_2O_3 was added to decrease the viscosity and aid glass formation and Sb_2O_3 was added as refining agent.

TABLE 1 Nominal glass composition

Oxide	(mol%)	(wt%)
Al_2O_3	17.67	26.15
SiO_2	55.52	48.41
ZrO_2	00.50	00.89
TiO_2	06.90	08.00
MgO	16.66	09.74
Sb_2O_3	01.25	05.29
B_2O_3	01.50	01.52

2.2 | Differential scanning calorimetry

Differential scanning calorimetry (DSC) analyses were conducted using a thermal analysis equipment (NETZSCH DSC 404, Selb, Bavaria, Germany) on both the powdered and bulk samples at a heating rate of 10 K/min from room temperature to 1473 K.

2.3 | Bulk X-ray diffraction and heat-treatment protocols

High-temperature X-ray diffraction (HTXRD) was conducted for the bulk samples using a D8 X-ray diffractometer (Bruker AXS, Billerica, MA, USA), using monochromatic Cu$K_{\alpha 1}$ radiation by means of an incident beam Ge monochromator, a Lynx Eye detector and a HTK1200 heating chamber (Anton Paar, Graz, Styria, Austria). The XRD patterns were recorded over the 10°-80° 2θ angular range, with a step of 0.02° 2θ, and an acquisition time of 0.5 seconds per step. For these experimental conditions, each diffractogram required approximately 30 minute to be recorded and 48 patterns were recorded during this heating step.

An initial run without any isothermal plateau was performed on a bulk sample and was conducted to identify which crystalline phases lead to the crystallization peaks shown in the DSC scan. Because no crystallization is expected below 773 K, the sample was heated from room temperature to 773 K at a fast rate of 9 K/min (no XRD pattern was recorded at this stage). From 773 to 1320 K a much slower heating rate of 0.42 K/min was applied.

A second analysis was conducted using two temperature plateaus (double-stage heat treatment). After applying different heat-treatment protocols (varying temperature and duration of the nucleation step and duration of the crystal growth step) to the parent glass, the hardness of the resulting glass-ceramics was measured. Hereafter, the optimum heat treatment that leads to a transparent glass-ceramic having the highest hardness was chosen to perform in situ measurements. This heat treatment is described as follows: the sample was heated from room temperature to 873 K at 7.2 K/min and then to 1006 K at 0.9 K/min. The temperature of 1006 K is the glass-transition temperature, T_g, as measured by DSC for a heating rate of 10 K/min. The sample was maintained at 1006 K for 48 hour to promote nucleation before being heated using a 2.7 K/min rate until the sample reached 1173 K. The sample was then held at this temperature for 10 hour to promote crystal growth. Each pattern was recorded over the 10°-80° 2θ range, with a step of 0.02° 2θ, and a step time of 0.5 s. The specimen was then rapidly cooled to room temperature. This heat-treatment protocol was also applied to the high-temperature in situ measurements of the elastic moduli.

2.4 | Mechanical properties

The room-temperature Young's modulus (E), shear modulus (G), and Poisson's ratio (ν) were calculated from acoustic wave velocities measured using ultrasonic echography with 10 MHz piezoelectric transducers powered with a DPR300 Pulse/Receiver (JSR Ultrasonics, Pittsford, NY, USA). Measurements were conducted using an oscilloscope (TDS3012 Tektronix, Beaverton, OR, USA). The ultrasonic velocities of the transverse (V_T) and longitudinal (V_L) acoustic waves were deduced from the transit time and the material thickness. The sample had a thickness of 8.26 ± 0.01 mm and a density of 2.822 ± 0.001 g/cm^3, as measured by the Archimedes method in distilled water. Values for E, G, and ν were calculated using the classical relationships[32]:

$$E = \rho\left[\frac{3V_L^2 - 4V_T^2}{\left(\frac{V_L}{V_T}\right) - 1}\right] \quad (1)$$

$$G = \rho V_T^2 \quad (2)$$

$$\nu = \frac{V_L^2 - 2V_T^2}{2(V_L^2 - V_T^2)} \quad (3)$$

In situ high-temperature measurements of E and G were performed in a sample that was manufactured using the temperature protocol described in section 2.3. Measurements were recorded during the entire heat-treatment. Values for E and G were calculated using flexural and torsional frequencies by resonance spectroscopy (RFDA, IMCE, Belgium) in a furnace (Nabertherm, Lilienthal, Lower Saxony, Germany) controlled by a software (RFDA HT1050). The sample dimensions were 25.20 mm × 43.55 mm × 3.57 mm. For a rectangular bar, the values of E and G are calculated as follows[33]:

$$E = 0.9465\left(\frac{mf_f^2}{b}\right)\left(\frac{L^3}{t^3}\right)T_1 \quad (4a)$$

$$T_1 = 1 + 6.585\left(1 + 0.0752v + 0.8109v^2\right)\left(\frac{t}{L}\right)^2 - 0.868\left(\frac{t}{L}\right)^4 - \left[\frac{8.340\left(1 + 0.2023v + 2.173v^2\left(\frac{t}{L}\right)^4\right)}{1 + 6.338\left(1 + 0.1408v + 1.536v^2\left(\frac{t}{L}\right)^2\right)}\right] \quad (4b)$$

$$G = \frac{4.L.m.f_t^2}{b.t}\left[\frac{B}{1+A}\right] \quad (5a)$$

$$A = \frac{\left[0.5062 - 0.8776\left(\frac{b}{t}\right) + 0.3504\left(\frac{b}{t}\right)^2 - 0.0078\left(\frac{b}{t}\right)^3\right]}{12.03\left(\frac{b}{t}\right) + 9.892\left(\frac{b}{t}\right)^2} \quad (5b)$$

$$B = \left[\frac{\frac{b}{t} + \frac{t}{b}}{4\frac{t}{b} - 2.52\left(\frac{t}{b}\right)^2 + 0.21\left(\frac{t}{b}\right)^6}\right] \quad (5c)$$

where E is the Young's Modulus (Pa), m is the sample mass (g), b is the width of the bar (mm), L is the length of the bar (mm), t is the thickness of the bar (mm), f_f is the fundamental flexural resonant frequency of the bar (Hz), f_t is the fundamental torsion resonant frequency of the bar (Hz), T_1 is a correction factor for the fundamental flexural mode to account for the finite thickness of the bar, and v is the Poisson's ratio. The values for E and G were used to calculate the Poisson's ratio according to the following relation:

$$\nu = \frac{E}{2G} - 1 \quad (6)$$

Both room and high-temperature measurements of E and G have associated errors of 1% of the measured value, due to the precision of the techniques.

3 | RESULTS

3.1 | DSC and in situ HTXRD analyses

Figure 1 shows the DSC traces for the bulk and powder samples. The coincidence of the curves is indicative of the copious internal nucleation that is desirable when crystallizing a glass to produce GC for technological applications due to the ease of microstructure control and reproducibility. The glass exhibits three crystallization peaks up to 1473 K, as shown in Figure 1. The glass-transition temperature, T_{gDSC}, obtained using the tangent rule is ≈1006 K.

Crystallization peaks appear at 1189, 1284, and 1441 K. Following the results of the initial HTXRD run (data not shown), the first peak corresponds to the precipitation of β-quartz (International Centre for Diffraction Data, ICDD PDF2 file 89-8951).

The second peak is broader and may correspond to the precipitation of three different crystalline phases that were detected in a 50 K-interval centered at the peak temperature: TiO_2 (ICDD PDF2 file 89-6975) at 1230 K, ringwoodite (γ-$2MgO{\cdot}SiO_2$, ICDD PDF2 file 74-1681) at 1243 K, and sapphirine ($4MgO{\cdot}5Al_2O_3{\cdot}2SiO_2$-ICDD PDF2 file 11-0607) at 1282 K. The crystalline phase responsible for the third crystallization peak was not detected due to the temperature limitation of the XRD diffractometer. Furthermore, heat treatments at this high temperature lead to softening of the specimens. Thus, such temperatures are not suitable to obtain glass-ceramics and were not further investigated.

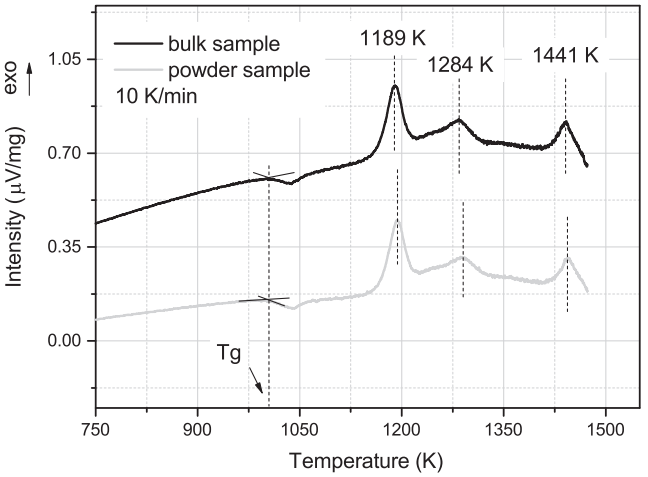

FIGURE 1 DSC analysis of the examined composition

After the nucleation stage at 1006 K for 2 days, the XRD pattern (not shown here) showed one peak at 2-θ=25.5° related to karooite ($MgO{\cdot}2TiO_2$) indicating that this phase is formed during the nucleation step. It is worth mentioning that the samples heat-treated at the crystallization temperature of 1173 K without prior nucleation treatment were opaque. This fact confirms that substantial crystal nucleation indeed occurs during that first step. The temperature was then raised to 1173 K, which is just below the first crystallization DSC peak. The crystal growth was monitored at this temperature for 10 hour. The XRD patterns collected during the first 92 minute and after 9 hour and 42 minute are shown in Figure 2A,B, respectively.

Five crystalline phases were identified after the first scan at 1173 K. One of the phases is magnesium spinel ($MgO.Al_2O_3$-ICDD PDF2 file 82-2424). This phase is known to be hard (H_v=15.4 GPa[34]), and its presence certainly enhances the hardness of the glass-ceramic. Sillimanite ($Al_2O_3{\cdot}SiO_2$) (ICDD PDF2 file 88-0892), with a hardness value of H_v ~11 GPa,[35] is also present. A third phase, karooite ($MgO{\cdot}2TiO_2$-ICDD PDF2 file 89-6944), formed during the nucleation step, has unknown hardness. Finally, due to its relatively high concentration in the glass, TiO_2 (H_v=7-11 GPa[36]) also precipitates. Because this first XRD scan required 30 minute to complete, it was not possible to distinguish which of the four phases appeared first. To distinguish the order of phase appearance, a faster scan could be used; however, this speed would compromise the already poor intensity of the peaks. Ultimately, sapphirine ($4MgO{\cdot}5Al_2O_3{\cdot}2SiO_2$-ICDD PDF2 file 11-0607)

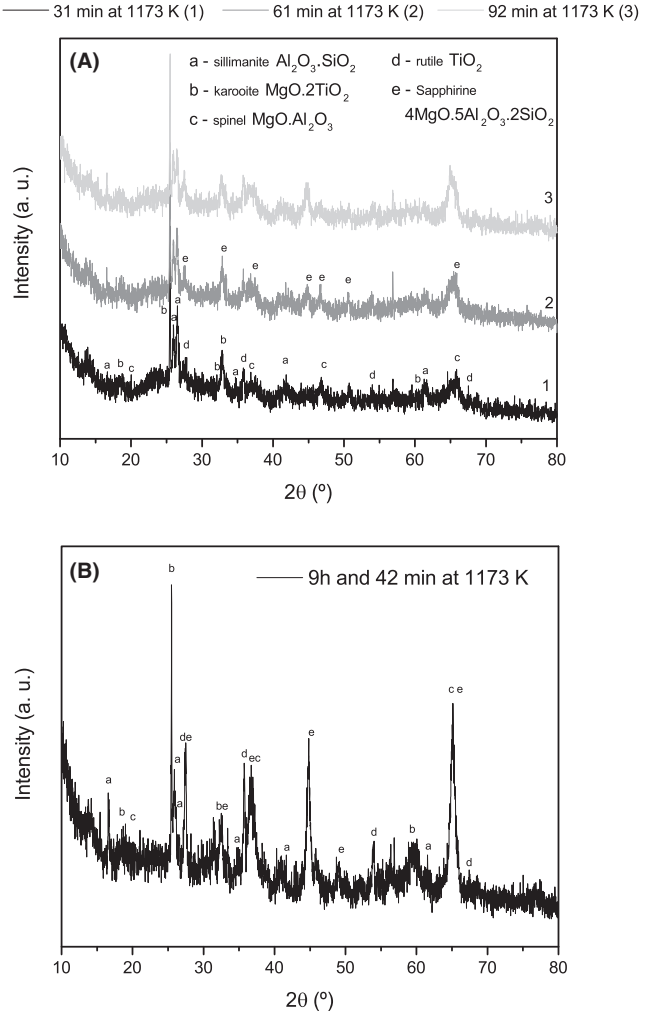

FIGURE 2 XRD patterns for the MAS glass, with a composition described in Table 1, nucleated for 48 h at 1006 K followed by (A) (from bottom to top) 31 min, 61 min and 92 min at 1173 K and (B) 9 h and 42 min at 1173 K. The identified crystal phases are: a-sillimanite ($Al_2O_3{\cdot}SiO_2$); b-karooite ($MgO{\cdot}2TiO_2$); c-spinel ($MgO{\cdot}Al_2O_3$); d-rutile (TiO_2); e-sapphirine ($4MgO{\cdot}5Al_2O_3{\cdot}2SiO_2$)

(H_v=13.3 GPa[37]) was also identified in the second scan, which started after 31 minute at 1173 K. Although the relative amounts of MgO, Al_2O_3, and SiO_2 in the parent glass lead exactly to the nominal composition of cordierite, the heat-treated glass—which had several other components added—lead at the treatment temperature of 1173 K, to the crystallization of sapphirine. The ternary equilibrium phase diagram shows that the sapphirine domain lies close to the nominal composition of cordierite, and the addition of B_2O_3, Sb_2O_3, TiO_2, and ZrO_2 to the parent glass likely dislocated the equilibrium, at this temperature, toward that domain. However, according to Höland and Beall[1] and Shao et al.,[12] heat treatments of similar glasses from the MAS system at temperatures higher than 1273 K, lead to the crystallization of cordierite. But for the purpose of this article, it is quite relevant to note that sapphirine has a higher Mohs hardness than cordierite. Hence, sapphirine containing glass-ceramics may be suitable for application as ballistic resistant materials. The third scan, which started after 61 minute, showed an increase in the intensities of all the diffraction peaks, including those attributed to sapphirine. Figure 2B shows the XRD pattern of the sample after 9 hours and 42 minute at 1173 K; the intensity of the peaks visibly increased, thus confirming that crystallization was not yet completed after 61 minute at this temperature.

It is also interesting to note that the thermal cycles of the DSC (10 K/min) and the HTXRD (variable rates) differ and thus, lead to the observation of crystalline phases at different temperatures. Also, the HTXRD heating protocol included a nucleation stage, that is, a temperature plateau (48 hour at 1006 K), which induced, as expected, glass crystallization at lower temperature when compared to the DSC analysis.

The role of TiO_2 in the crystallization of cordierite ($2MgO{\cdot}2Al_2O_3{\cdot}5SiO_2$) in MAS glassy systems has been extensively discussed. It is classically assumed that TiO_2 induces liquid-liquid phase separation in the volume of MAS glasses that triggers crystal nucleation. Then, the Ti-rich liquid crystallizes as a Ti-containing phase. This phase is, thus, used as a substrate for the crystallization of cordierite.[12,15,17] However, the hypothesis of liquid-liquid phase separation for the crystallization of cordierite is not the only one that has been proposed. For instance, Guignard et al.[38] have shown that titania promotes nucleation through the formation of highly coordinated Al species and structural fluctuations on the glass that emulates the precipitating crystal phase. This hypothesis does not exclude the previous nucleation of a TiO_2-enriched phase. In this study, one peak related to karooite is present in the XRD pattern taken at the nucleation step (XRD not presented), indicating that sapphirine, which, among all discussed crystalline phases, has the most similar chemical composition to cordierite, might have used karooite ($MgO{\cdot}2TiO_2$) as nucleation site. Also, in accordance to Sato,[39,40] sapphirine may have crystallized on the expense of spinel. No crystalline phase containing ZrO_2 was detected in the in situ HTXRD experiments with two temperature steps. This means that ZrO_2-containing crystals are either present in a nondetectable quantity (which is quite possible), or that Zr remains dissolved in the residual glass.

3.2 | Temperature dependence of the elastic properties up to the crystallization plateau

The elastic properties of the glass at room temperature were assessed using ultrasonic echography. By applying Equations (1), (2) and (3), values of $E = 106 \pm 8$ GPa, $G = 42 \pm 2$ GPa and $\nu = 0.27 \pm 0.02$ were obtained.

To observe the evolution of these elastic properties during heat treatment, a glass sample was submitted to the same temperature processing used for the HTXRD analysis. Values of E and G were then calculated using the method described in section 2.4. An overview of the temperature variation over time is presented in Figure 3 along with the evolution of the shear modulus.

Figure 4 shows the variation in the mechanical properties, E, G and ν, for temperatures up to 1173 K. The experimental points were fitted using different equations. At $T<T_{gM}$, where T_{gM} is the glass-transition temperature deduced from the variation in $E(T)$ or $G(T)$, the temperature dependence of the elastic moduli is well described by the expression proposed by Wachtman[41] (Equation 7):

$$M = M_{0K} - BT\exp\left(\frac{-T_0}{T}\right) \tag{7}$$

where M is the elastic modulus (E or G) and M_{0K} is the value when approaching 0 K. The variables B and T_0 are fitting parameters. This expression was used to fit the experimental points between 1007 and 1035 K, as shown in Figure 4.

For temperatures between T=1045 K and the DSC crystallization temperature, T_x (1173 K), a power law expression (Equation 8) is more suitable[42]:

$$\left(\frac{M}{M\left(T_g\right)}\right) = \left(\frac{T_g}{T}\right)^{\alpha_M} \tag{8}$$

where α_M may range from 0.07 for amorphous SiO_2 to 10 for amorphous Se[42] and is related to how fast the liquid softens with temperature. This value is therefore correlated with the fragility index, as described by the concept introduced by Angell.[43] In this expression, $M\left(T_g\right)$ and α_M are

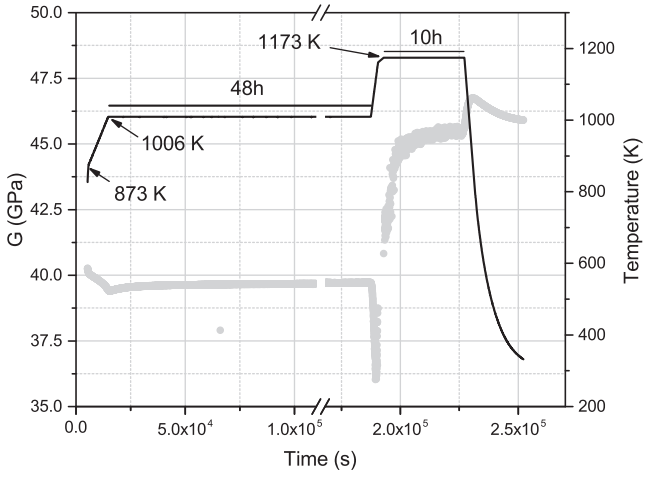

FIGURE 3 Overview of the temperature variation over time in the in situ measurements of the mechanical properties and the time dependence of the shear modulus during the entire experiment

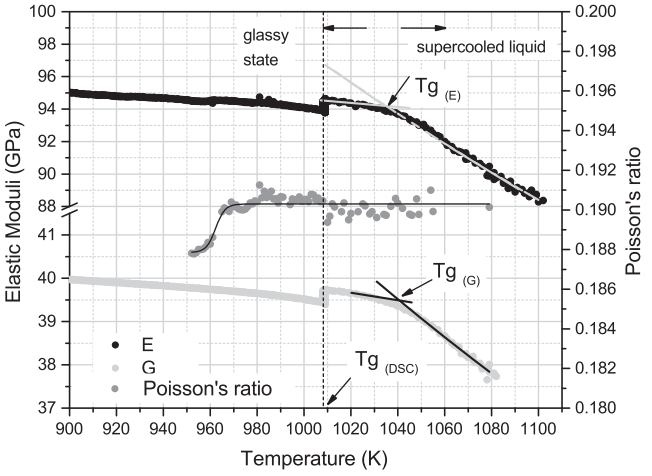

FIGURE 4 The temperature dependence of E, G and ν for two monotonic heating experiments with a plateau at T_{gDSC} between them. Full lines over the experimental points for E and G represent fitting using Equation (7) for $T<T_{gM}$ and Equation (8) for $T>T_{gM}$. The full line over the calculated Poisson's coefficient is used as a guide. The sample was heated from room temperature to 873 K at 7.2 K/min and then to 1006 K at 0.9 K/min. The sample was maintained at 1006 K for 48 h to promote nucleation, then heated using a 2.7 K/min rate until 1173 K. The sample was then held at this temperature for 10 h to promote crystal growth

obtained using a fitting procedure. For fitting purposes, we used $T_g = T_{gDSC}$(1006 K).

Equations (7) and (8) satisfy two fundamental requirements: (i) $\left.\frac{dM}{dT}\right|_{solid}$, approaches zero as T approaches 0 K and (ii) $\left.\frac{dM}{dT}\right|_{liquid}$, approaches zero as T tends to the maximum temperature sustainable by the melt ($T_{vaporization}$).

In Figure 4, the glass-transition range, T_{gG} and T_{gE}, associated with the mechanical resonance is located where the curves corresponding to the glassy and liquid states (Equations 7 and 8, respectively) intersect. Note that T_{gG} and T_{gE} were calculated from $E(T)$ and $G(T)$ after a 48-hour nucleation plateau during which karooite nucleated. Therefore, without the nucleation plateau, T_{gE} and T_{gG} would be different and may be closer to T_{gDSC}.

Table 2 shows the following: glass transition temperature after the nucleation treatment, T_{gE} and T_{gG}, the E, G, and ν values at room temperature, the softening rates for E and G immediately below and above T_g (dE/dT^- (T_{gE}), dE/dT^+ (T_{gE}), dG/dT^- (T_{gG}) and dG/dT^+ (T_{gG}), respectively) obtained through the derivation of Equations (7) and (8), and the α_E and α_G values. As a comparison, some typical data for different glasses were added.[42,44–46]

Although Poisson's ratio (ν) is a coefficient associated with the elastic properties at the macroscopic scale, it has been previously shown[30] to be linked to atomic network connectivity. The values of ν typically range from 0.1 (for

TABLE 2 Elastic properties of the investigated glass and glass-ceramics and glasses of similar compositions

	E (297 K) (GPa)	G (297 K) (GPa)	ν (297 K)	T_g (E) (K)	T_g (G) (K)	dE/dT^- (T_{gE}) (MPa·K^{-1})	dE/dT^+ (T_{gE}) (MPa·K^{-1})	dG/dT^- (T_{gG}) (MPa·K^{-1})	dG/dT^+ (T_{gG}) (MPa·K^{-1})	α_E	α_G
This study	98.1	41.3	0.187	1035	1041	−12.5	−94.8	−8	−45	1.04 ± 0.03	1.18 ± 0.02
Alumi. Sil. 1[a]	—	—	—	933	940	−9.3	−62.6	−4.8	−25.9	0.77 ± 0.01	0.81 ± 0.01
Alumi. Sil. 2[b]	—	—	—	939	935	−15.7	−52.4	−6.1	−23.5	0.66 ± 0.02	0.73 ± 0.02
Alumi. Sil. 3[c]	84.0	33.5	0.25	968	960	−11.3	−67.3	−5.3	−29.1	0.83 ± 0.01	0.90 ± 0.01
Alumi. Sil. 4[d]	87.6	34.8	0.26	1012	1019	−6.7	−53.4	−4.7	−24.7	0.64 ± 0.03	0.78 ± 0.03
Grossular[e]	92.1	36.0	0.28	1077	1074	−11.3	−73.8	−4.5	−30.5	0.95 ± 0.06	1.00 ± 0.07
Anorthite[f]	—	—	—	1141	1124	−13.9	−43.2	−3.8	−18.1	0.55 ± 0.01	0.57 ± 0.01
Window Glass	72.0	29.5	0.22	852	855	−28.8	−70.6	−12.6	−29.7	0.93 ± 0.03	0.97 ± 0.03
Diopside[g]	97.5	38.3	0.27	1218	1276	−32.1	−62.6	−22.7	−14.4	1.00 ± 0.04	1.04 ± 0.02

[a]Al/Si=0.29.
[b]Al/Si=0.36.
[c]Al/Si=0.35.
[d]Al/Si=0.5.
[e]$Ca_3Al_2Si_3O_{12}$.
[f]$CaAl_2Si_2O_8$.
[g]$CaMgSi_2O_6$.

a highly polymerized structure, such as silica glass) to 0.4 (for a weakly polymerized structure containing a high percentage of nonbridging oxygen).[30] Vitreous silica (v-SiO_2) has a highly cross-linked network (Q^4 structure) and a small value of ν. The glass studied in this work has a nominal composition that corresponds to 75 mol% cordierite ($2MgO{\cdot}2Al_2O_3{\cdot}5SiO_2$), and hence the structure of the glass should consist mostly of Q^3 units, which also leads to a cross-linked structure. These results explain the relatively low values of ν observed. The studied glass possesses the largest shear modulus value and the third highest T_g among all the glasses in Table 2; these findings are consistent with a highly cross-linked structure having a strong atomic binding energy.

However, the studied glass also exhibits the highest softening rate below and above T_g (dG/dT^- (T_{gG}) and dG/dT^+ (T_{gG})) and the largest α_G.[47] This liquid is therefore classified as being relatively fragile. One possible explanation is the composition of the crystalline phases acting as nuclei. As shown in Figure 2A, Mg-spinel, rutile, karooite, and sillimanite are present in the early stages at 1173 K. Because these phases are stable at high temperatures and have a high bonding energy, the residual glassy phase remaining after the crystallization treatment is expected to be less refractory than the parent pristine glass. The residual glassy phase is likely to govern the softening stage and is responsible for the fragile-like character of the liquid. The nuclei act as stiff "islands" (crystalline phases having high values of E and G) that are weakly interconnected by the residual glassy phase.[42]

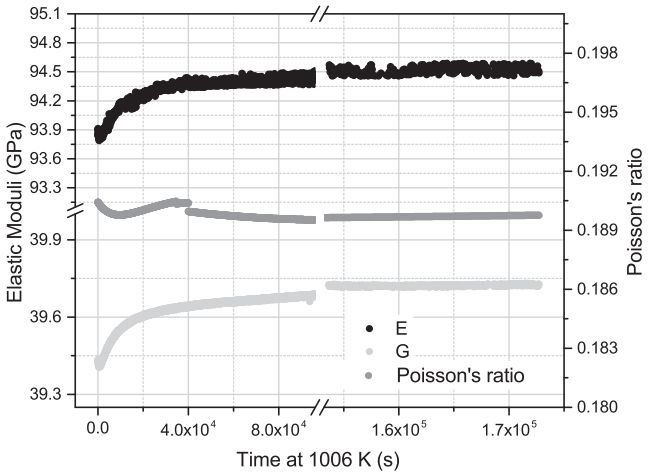

FIGURE 5 Young's modulus (E), shear modulus (G), and Poisson's ratio (ν) as a function of the annealing time at 1006 K for the investigated glass composition

3.3 | Isothermal evolution of elastic properties

3.3.1 | At the nucleation range

Figure 5 shows the evolution of E, G, and ν during the 48-hour nucleation treatment at 1006 K.

In the first ten hours of annealing at 1006 K, E and G exhibit monotonic and significant increases, which are attributed to some degree to the crystallization of karooite. For longer times, only a slight evolution is observed (less than a 0.5% increase in E). Nucleation must have a minor

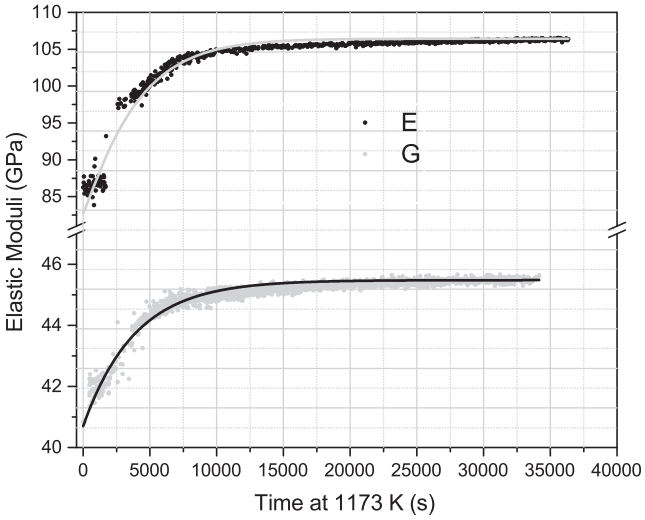

FIGURE 6 Experimental points for the Young modulus, shear modulus and the evolution of the crystalline volume fraction, given by the JMAK equation, at the 10 h crystallization step at 1173 K

effect on the overall atomic connectivity and packing density, thus the effect of the nucleation treatment on ν is very limited (if any). As observed in Figure 3, for the initial stage of nucleation, there is a decrease in *G*. At 1006 K, the glass starts to relax, which promotes a decrease in the mechanical properties. When the crystallized volume fraction increases, it promotes increases in *E* and *G*, as indeed observed.

3.3.2 | Evolution of the elastic moduli during crystallization

Figure 6 shows the evolution of *E*, *G* and ν during the crystallization treatment at 1173 K. The experimental data could be smoothly fitted using the rule of mixtures for the effective moduli of the developing glass-ceramic material, given by Equation (9). The evolution of the crystallized volume fraction is described by the Johnson-Mehl-Avrami-Kolmogorov equation. The evolution of the elastic moduli is given by (Equation 9)[48]:

$$M_{GC} = (1 - f(t))M_{RG} + (1 - (\exp(-Kt^n))M_C \qquad (9)$$

where M_{GC} is the elastic modulus (*E* or *G*) of the glass-ceramic, M_{RG} is the elastic modulus (*E* or *G*) of the residual glass, taken at *t*=0 second at 1173 K, and M_C is the elastic modulus of the crystalline phase, taken at *t*=10 hour at 1173 K. The variable *K* is a constant at any temperature, and *n* is the Avrami index an integer or half-integer. Table 3 summarizes the parameters used to fit the experimental data obtained for *E* and *G*, as well as the obtained values of *K* and *n*. The errors of *K* and *n* were estimated using the least-squares method. The value of *n* for crystallization from a fixed number of nuclei can be 1 or 0.5 for needlelike crystals, 2 or 1.5 for flat crystals, and 3 or 2.5 for spherical or cubic crystals.[49] The values of *n* obtained by fitting, 1.11 ± 0.02 (fitting of *E*) and 1.00 ± 0.01 (fitting of *G*), suggest that the majority of the crystals exhibit a needlelike shape geometry.

TABLE 3 Values of elastic properties (E_{RG} and G_{RG}, E_c and G_c) used to fit the experimental data of *E* and *G* (Figure 7) as well as obtained values of *k* and *n*

E_{RG} (GPa)	E_C (GPa)	*K*	*n*
82.7 ± 0.1	106.4 ± 0.1	$1 \times 10^{-4} \pm 1 \times 10^{-5}$	1.11 ± 0.02
G_{RG} (GPa)	G_C (GPa)	*K*	*n*
40.7 ± 0.1	45.5 ± 0.1	$3 \times 10^{-4} \pm 2 \times 10^{-5}$	1.00 ± 0.01

Figure 7 shows the evolution of the Poisson ratio during the crystallization stage at 1173 K.

At the beginning of the crystallization process, the volume fraction of the nuclei is extremely low, and hence the volume fraction of the glass matrix is very high. Because the glass has a more open structure compared to the crystal, the Poisson's ratio is low in the early stages at 1173 K and increases as the crystallized fraction increases. As crystallization evolves, the atomic packing density (C_g) increases, leading to an increase in ν.[30]

The time-dependent elastic curves (Figure 6) show that the mechanical properties increase only slightly between 10 000 seconds (2 hour and 47 minute) and 15 000 seconds (4 hour and 10 minute) of crystallization treatment. This increase suggests that there is only a small change in the crystallized volume fraction over this time interval, which is confirmed by the X-ray patterns (not shown here) that show no difference in peak intensity after 10 000 and 15 000 seconds. However, the change is detected by a continuous increase in Poisson's ratio, which becomes constant

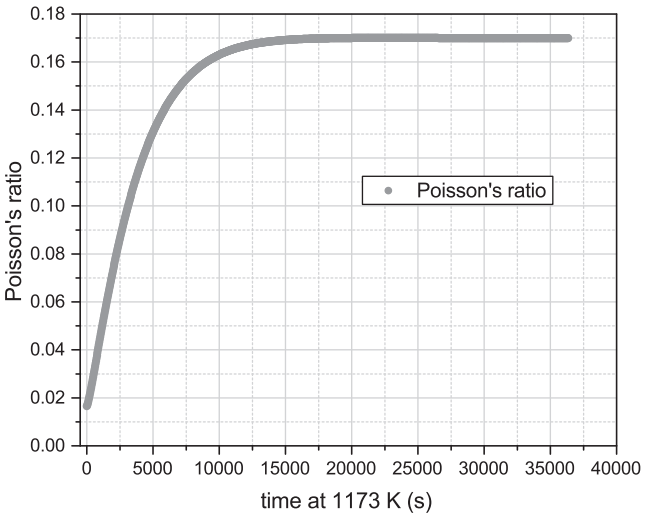

FIGURE 7 Poisson's ratio at the 10 h crystallization step at 1173 K

only after 15 000 seconds. The slow evolution of the composition and the network structure of the residual glassy phase over the next 3 hour were reflected by the increase in ν up to 15 000 seconds. After this specific crystallization cycle, a transparent glass-ceramic containing five crystalline phases (karooite, spinel, sillimanite, rutile, and sapphirine) was obtained.

The obtained glass-ceramics were ballistic tested in a Brazilian Air Force research facility in São José dos Campos, Brazil. The results (to be presented on an incoming paper) were promising, showing a ballistic resistance similar to that of a transparent aluminum-oxynitrate (AlON) and polycrystalline Al_2O_3.

4 | SUMMARY AND CONCLUSIONS

In this work, we followed the in situ evolution with temperature of crystal phases and three mechanical properties of a ballistic resistant armor glass-ceramic. The elastic moduli and Poisson's ratio were studied as a function of temperature and time.

The elastic moduli decrease with increasing temperature, up to 1173 K. The values of the Poisson's ratio during this heating cycle indicate a highly linked structure that quickly softens with increasing temperatures, as indicated by an α value that is typical of a fragile glass. The isothermal evolution of the elastic moduli during the nucleation step at 1006 K shows a more pronounced increase in the values of *E* and *G* during the first 10 hour, as the crystal nuclei appear. As time progresses, those properties still change, although at a slower rate. At the crystallization stage at 1173 K, elastic properties evolve faster during the first 2 hours. Crystallization leads to an increase in approximately 20% in the elastic moduli.

The first crystalline phase formed was karooite ($MgO{\cdot}2TiO_2$), which was detected during the nucleation stage at 1006 K for 2 days. After 31 minute of the subsequent heat treatment at 1173 K, four crystalline phases were identified Mg-spinel, rutile, karooite, and sillimanite. Sapphirine crystallizes after those four phases, indicating that karooite might have act as a nucleating agent. After the above described crystallization cycle, a transparent glass-ceramic was obtained.

ACKNOWLEDGMENTS

The authors thank the São Paulo State Research Foundation - FAPESP for the financial support of L. S. Gallo (BEPE Grant 2014/03004-0) during his stay at the Department of Mechanics and Glasses at the University of Rennes 1 and also for the funding of the Center for Research, Technology and Education in Vitreous Materials (FAPESP CEPID Process 2013/07793-6), where a portion of the presented experiments were conducted. Tanguy Rouxel is grateful to the European Research Council for supporting these studies through the Advanced Grant 320506 (DAMREG) of the 7th framework program "Ideas".

REFERENCES

1. Höland W, Beall GH, *Glass Ceramic Technology*, 2nd edn. Westerville: The American Ceramic Society; 2012.
2. Peitl O, Zanotto ED, Serbena FC, Hench LL. Compositional and microstructural design of highly bioactive P_2O_5–Na_2O–CaO–SiO_2 glass-ceramics. *Acta Biomater*. 2012;8:12.
3. Crovace MC, Souza MT, Chinaglia CR, Peitl O, Zanotto ED. Biosilicate® — A multipurpose, highly bioactive glass-ceramic. In vitro, in vivo and clinical trials. *J Non-Cryst Solids*. 2016;432:20.
4. Klyukin DA, Sidorov AI, Ignatiev AI, Nikonorov NV. Luminescence quenching and recovering in photo-thermo-refractive silver-ion doped glasses. *Opt Mater*. 2014;38:5.
5. Hench LL, *An Introduction to Bioceramics*, 2nd edn. London:: Imperial College Press; 2013:620.
6. Rudoi BL. *Ballistic Resistant Glass-Ceramic and Method of Preparation*, Vol. 4473653, pp. 8. Alexandria: U. S. P. Office; 1984.
7. Beall GH. *Glass-Ceramic Bodies and Method of Making Them*, Vol. 3,252,811, pp. 7. Alexandria: U. S. P. Office. Corning Glass Works; 1966.
8. Budd MI, Darrant JG. *Glass-Ceramic Armour*, Vol. 2284655, pp. 16. Newport: I. P. Office. GEC Alsthom; 1995.
9. Hunger A, Carl G, Rüssel C. Formation of nano-crystalline quartz crystals from ZnO/MgO/Al_2O_3/TiO_2/ZrO_2/SiO_2 glasses. *Solid State Sci*. 2010;12:5.
10. Fokin VM, Zanotto ED, Yuritsyn NS, Schmelzer JWP. Homogeneous crystal nucleation in silicate glasses: a 40 years perspective. *J Non-Cryst Solids*. 2006;352:33.
11. Serbena FC, Mathias I, Foerster CE, Zanotto ED. Crystallization toughening of a model glass-ceramic. *Acta Mater*. 2015;86:13.
12. Shao H, Liang K, Zhou F, Wang G, Hu A. Microstructure and mechanical properties of MgO–Al_2O_3–SiO_2–TiO_2 glass–ceramics. *Mater Res Bull*. 2005;40(3):7.
13. Sung Y-M. Mechanical properties of α-cordierite and β-spodumene glass-ceramics prepared by sintering and crystallization heat treatments. *Ceram Int*. 1997;23(5):6.
14. Chen G-H, Liu X-Y. Sintering, crystallization and properties of MgO–Al_2O_3–SiO_2 system glass-ceramics containing ZnO. *J Alloy Compd*. 2007;431:4.
15. Shao H, Liang K, Peng F. Crystallization kinetics of MgO–Al_2O_3–SiO_2 glass-ceramics. *Ceram Int*. 2004;30:4.
16. Yang C-F. The mechanical properties of MgO-CaO-Al_2O_3–SiO_2 composite glass. *Mater Sci Eng: C*. 1997;4:5.
17. Goel A, Shaaban ER, Melo FCL, Ribeiro MJ, Ferreira JMF. Non-isothermal crystallization kinetic studies on MgO– Al_2O_3–SiO_2–TiO_2 glass. *J Non-Cryst Solids*. 2007;353:2383–2391.
18. Cormier L, Dargaud O, Menguy N, et al. Investigation of the role of nucleating agents in MgO-SiO_2-Al_2O_3-SiO_2-TiO_2 glasses and glass-ceramics: a XANES study at the Ti K- and L2,3-edges. *Cryst Growth Des*. 2011;11:9.
19. Dargaud O, Calas G, Cormier L, et al. In situ study of nucleation of zirconia in an MgO–Al_2O_3–SiO_2 glass. *J Am Ceram Soc*. 2010;93:3.

20. Cormier L, Dargaud O, Calas G, et al. Zr environment and nucleation role in aluminosilicate glasses. *Mater Chem Phys*. 2015;152:7.
21. Wang S-M, Kuang F-H, Yan Q-Z, Ge C-C, Qi L-H. Crystallization and infrared radiation properties of iron ion doped cordierite glass-ceramics. *J Alloy Compd*. 2011;509:5.
22. Marghussian VK, Balazadegan O, Eftekhari-yekta B. Crystallization behaviour, microstructure and mechanical properties of cordierite–mullite glass ceramics. *J Alloy Compd*. 2009;484:902–906.
23. Medvedovski E. Alumina ceramics for ballistic protection, Part 1. *Am Ceram Soc Bull*. 2002;81(3):6.
24. Stookey SD. *Ceramic Body and Method of Making It*. USA: U. P. a. T. Office. Corning Glass Works; 1961:6.
25. Takagi K, Tashiro M. *Method of Preventing Scum Formation in Glass Melts, and Glass-Ceramic Products*. USA: U. P. a. T. Office. Nippon Electric Glass Co; 1966:3.
26. Bolton N, Smith WN. *Fire Resistant Transparent Laminates*. USA: U. P. O. a. Trademark. Artistic Glass Products Company; 1996.
27. Darrant JG, Thompson CA. *Processing of Transparent Glass-Ceramic*. Alstom: W. I. P. Organization; 2003: 28.
28. Guazzato M, Albakry M, Ringer SP, Swain MV. Strength, fracture toughness and microstructure of a selection of all-ceramic materials. Part II. Zirconia-based dental ceramics. *Dent Mater*. 2004;20:8.
29. Dittmer M, Rüssel C. Colorless and high strength $MgO/Al_2O_3/SiO_2$ glass–ceramic dental material using zirconia as nucleating agent. *J Biomed Mater Res, Part B*. 2012;100B:8.
30. Rouxel T. Elastic properties and short-to medium-range order in glasses. *J Am Ceram Soc*. 2007;90:20.
31. Fokin VM, Zanotto ED. Surface and volume nucleation and growth in TiO_2–cordierite glasses. *J Non-Cryst Solids*. 1999;246:13.
32. Keryvin V, Vaillant M-L, Rouxel T, Huger M, Gloriant T, Kawamura Y. Thermal stability and crystallisation of a $Zr_{55}Cu_{30}Al_{10}Ni_5$ bulk metallic glass studied by in situ ultrasonic echography. *Intermetallics*. 2002;10:8.
33. ASTM International. *Standard Test Method for Dynamic Young's Modulus, Shear Modulus, and Poisson's Ratio by Impulse Excitation of Vibration*. West Conshohocken: ASTM International; 2009:16.
34. Barthelmy D ed. Spinel mineral data. In: *Mineralogy Database*. 2015, http://webmineral.com/data/Spinel.shtml#.VTeNTyGqqko Accessed May 4, 2015.
35. Barthelmy D ed. Sillimanite mineral data. In: Barthelmy D, ed. *Mineralogy Database*. 2015, http://webmineral.com/data/Sillimanite.shtml#.V1CBKZErLIU. Accessed May 3, 2015.
36. Barthelmy D, ed. Rutile Mineral Data. In: *Mineralogy Database*. 2015, http://webmineral.com/data/Rutile.shtml#.WJTpnvkrLIU. Accessed May 3, 2015.
37. Barthelmy D. Sapphirine Mineral Data. In: *Mineralogy Database*. 2015, http://webmineral.com/data/Sapphirine.shtml#.WJTpwfkrLIV. Accessed May 1, 2015.
38. Guignard M, Cormier L, Montouillout V, Menguy N, Massiot D. Structural fluctuations and role of Ti as nucleating agent in an aluminosilicate glass. *J Non-Cryst Solids*. 2010;356:5.
39. Sato K, Miyamoto T, Kawasaki T. Experimental calibration of sapphirine–spinel Fe^{2+}–Mg exchange thermometer: implication for constraints on P-T condition of Howard Hills, Napier Complex, East Antarctica. *Gondwana Res*. 2006;9:11.
40. Sato K, Miyamoto T, Kawasaki T. Experimental constraints of metamorphic pressure and temperature, and phase relations of a phlogopite-orthopyroxene granulite from Howard Hills, Napier Complex, East Antarctica. *J Miner Petrol Sci*. 2004;99:11.
41. Wachtman JB, Tefft WE, Lam DG, Apstein CS. Exponential temperature dependence of young's modulus for several oxides. *Phys Rev*. 1961;122:6.
42. Rouxel T. Thermodynamics of viscous flow and elasticity of glass forming liquids in the glass transition range. *J Chem Phys*. 2011;135:15.
43. Angell CA. Perspective on the glass transition. *J Phys Chem Solids*. 1988;49(8):8.
44. Huger M, Chotard T, Internal Report. Limoges: Université de Limoges.
45. Gueguen Y, Rouxel T, Gadaud P, Bernard C, Keryvin V, Sangleboeuf J-C. High-temperature elasticity and viscosity of Ge_xSe_{1-x} glasses in the transition range. *Phys Rev B*. 2011;84:8.
46. Askarpour V, Manghnani MH, Richet P. Elastic properties of diopside, anorthite, and grossular glasses and liquids: a brillouin scattering study up to 1400 K. *J Geophys Res*. 1993;98:6.
47. Angell CA. Simulation of glasses and glass-forming liquids after two decades: some perspectives. *Comput Mater Sci*. 1995;4:6.
48. Weinberg MC, Birnie DP III, Shneidman VA. Crystallization kinetics and the JMAK equation. *J Non-Cryst Solids*. 1997;219:11.
49. Zanotto ED, Galhardi A. Experimental test of the general theory of transformation kinetics: homogeneous nucleation in a $Na_2O{\cdot}2CaO{\cdot}3SiO_2$ glass. *J Non-Cryst Solids*. 1988;104:8.

How to cite this article: Sant'Ana Gallo L, Célarié F, Audebrand N, Martins Rodrigues AC, Dutra Zanotto E, Rouxel T. In situ crystallization and elastic properties of transparent $MgO–Al_2O_3–SiO_2$ glass-ceramic. *J Am Ceram Soc*. 2017;00:1–10.